Kinetic study of biomass char combustion in a low temperature fluidized bed reactor

Mathieu Morin, Sébastien Pécate, Mehrdji Hemati

Kinetic study of biomass char combustion in a low temperature fluidized bed reactor

Mathieu Morin*, Sébastien Pécate, Mehrdji Hémati

Laboratoire de Génie Chimique, Université de Toulouse, CNRS, INPT, UPS, 4 allée Emile Monso, 31432 Toulouse, France

Keywords:
Combustion
Fluidized bed
Char
Kinetic
TGA

A B S T R A C T

The purpose of this work is the kinetic study of biomass char combustion in a low temperature fluidized bed reactor. This char was obtained from fast pyrolysis of beech stick in an annex batch fluidized bed reactor at 923 K and atmospheric pressure. Operating conditions of the combustion were thoroughly characterized so that the reaction takes place in isothermal conditions and a constant oxygen partial pressure. The kinetic study was performed for temperatures up to 643 K, oxygen partial pressures ranging from 5065 to 21273 Pa and cylindrical char particles (D = 4 mm and L = 9 mm). The Volumetric Model was found to be in very good agreement with experimental data. Values of activation energy and reaction order with respect to oxygen are respectively equal to 144 kJ/mol and 0.59. The reaction scheme during char combustion showed that char first reacts with oxygen to form CO which is further oxidized either at the particle surface or in the gas phase to produce CO_2. Besides, it was found that the char reactivity in combustion is higher in a fluidized bed reactor compared to TGA. This was explained by diffusional effects of oxygen and CO oxidation within the crucible in the TGA.

1. Introduction

Biomass is a possible alternative to the direct use of fossil fuel in gasification process as it has the advantage of being neutral in regard to the CO_2 emissions considering photosynthesis reactions. Biomass gasification produces synthesis gas which can be directly burned for heat and electricity production or used as a feedstock for the production of methane via Methanation process or liquid via Fisher Tropsch process. Biomass gasification is a thermochemical conversion occurring at high temperatures with many simultaneous reactions. It occurs in two stages: (i) for temperatures above 623 K, biomass undergoes a fast thermal conversion. This pyrolysis step converts the biomass into volatile products either condensable (steam and tars) or non condensable (H_2, CO, CO_2, CH_4 and C_2H_x) and a solid residue called char [1]; (ii) for temperatures greater than 973 K, the char reacts with steam and carbon dioxide. This gasification step converts the char into synthesis gas.

The reactive system of biomass conversion (i.e. pyrolysis + gasification) is an endothermic process. A contribution of energy is necessary in order to maintain the temperature and the different reactions in the reactor. Two types of technologies exist for biomass gasification according to the method of heat transmission [2]. Firstly, the heat can be supplied by partial combustion of the fuel in the gasifier itself. This process includes the fixed bed gasifiers (co and counter current) and the “bubbling fluidized bed” gasifiers. Secondly, the heat can be provided from a source outside of the gasifier by external heat (plasma or solar) or internal recirculation of gas and char. In the latter approach, Fast Internally Circulating Fluidized Bed (FICFB) [3] is currently a promising process which uses a circulation of a medium between an entrained bed exothermic reactor and a dense endothermic reactor. In the exothermic reactor called combustor, a part of the char from the gasifier is burnt and heats the medium. In the endothermic reactor called gasifier, the medium provides the heat necessary for the biomass gasification.

During biomass gasification in dual fluidized bed, the char reacts with steam and carbon dioxide in the gasifier and with oxygen in the combustor. Information regarding the kinetic of char combustion in a fluidized bed reactor is then essential to better understand phenomena inside a combustor.

The char combustion proceeds in several steps: the external transfer of oxygen from the bulk to the external surface of the particle, the diffusion of oxygen within the pores of the solid, the oxygen chemisorption on an active site (adsorption), the intrinsic chemical reaction and finally the products desorption [4,5]. Together, these different steps are strongly affected by the physicochemical properties of the char, the combustion temperature, the oxygen partial pressure, the size of the solid char particles and the type of reactor.

The physicochemical properties and the reactivity of biomass char depend on the pyrolysis operating conditions. This has been discussed

* Corresponding author.
E-mail addresses: mathieu.morin18@gmail.com (M. Morin), sebastien.pecate@ensiacet.fr (S. Pécate), mehrdji.hemati@ensiacet.fr (M. Hémati).

http://dx.doi.org/10.1016/j.cej.2017.08.063

Nomenclature

A_{VM}	pre exponential factor for the Volumetric model ($Pa^{-n}.s^{-1}$)
$C^s_{O_2}$	oxygen concentration at the surface of the char particles ($mol.m^{-3}$)
$C_{O_{2,i}}$	oxygen concentration at the CSTR outlet i ($mol.m^{-3}$)
E_a	activation energy ($J.mol^{-1}$)
$f(X)$	structure function ( )
H	height of the crucible (m)
K_c	global mass transfer coefficient (m/s)
n	reaction order with respect to oxygen ( )
$n_{char,crucible}$	initial amount of char in the crucible (mol)
$(n_{carbon})_{char}$	initial amount of carbon in 2.2 g of STI650 (mol)
$\dot{n}_t(t)$	instantaneous total molar flow rate ($mol.s^{-1}$)
$\dot{n}_i(t)$	instantaneous partial molar flow rate of component i ($mol.s^{-1}$)
$P_{O_{2,s}}$	oxygen partial pressure at the particle surface (Pa)
R	universal gas constant ($J.mol^{-1}.K^{-1}$)
R_{app}	apparent reaction rate at X = 0.5 (s^{-1})
$S_{crucible}$	crucible surface (m^2)
t_f	final time of the combustion (s).
T_p	particle temperature (K)
$w(t)$	instantaneous sample weight (kg)
w_{ash}	final sample weight (kg)
w_i	initial sample weight (kg)
X	conversion rate ( )
X_c	carbon conversion rate ( )
$x_i(t)$	molar fraction of component i ( )
$Y^i_{H_2}$	normalized fraction of hydrogen at the outlet of CSTR i ( )

Greek letters

δ_c	height of the char layer in the crucible (m)
ε	porosity of the char layer in the crucible ( )
ε_p	particle porosity ( )
ρ_a	apparent density ($kg.m^{-3}$)
ρ_t	true density of the char particle ($kg.m^{-3}$)
τ	tortuosity of the char layer $\tau = \sqrt{2}$ ( )
τ_{CSTR}	residence time of the CSTR (s)

in a previous paper [6]. It was shown that the pyrolysis operating conditions such as the heating rate, the pyrolysis temperature and the biomass nature strongly influence the amount of hydrogen, oxygen, carbon and ash content in the char as well as the presence of aromatic and amorphous carbons. Besides, a raise of the heating rate during biomass pyrolysis increases the char reactivity while a raise of the final pyrolysis temperature decreases the reactivity. The amount of ash in the char matrix may also catalyze the reaction of combustion.

The reaction of combustion can be divided into three main regimes according to the temperature, the oxygen partial pressure and the char particles size [5]. In Regime I (i.e. low temperatures), the intrinsic chemical reaction is low with respect to oxygen diffusion inside the pores and external transfer around the particle. The intrinsic chemical reaction is the limiting step. The Regime II (i.e. medium temperatures regime) is the transition regime where both the intrinsic chemical re action and the diffusion of oxygen play a significant role. In Regime III (i.e. high temperatures regime), the intrinsic reactivity of the solid is very high and oxygen molecules react as soon as they have passed the boundary layer around the particle. External mass transfer is then the limiting step. Consequently, to determine char O_2 combustion kinetic, many authors [7 9] minimized mass and heat transfers by carefully choosing the combination of combustion temperature, oxygen partial pressure and particles size so that the combustion occurs in the che mical control regime (i.e. Regime I).

The char combustion is highly dependent on the combustion tem perature and the oxygen partial pressure. It is well known in the lit erature that the combustion rate increases by raising these two para meters [7,8,10 15]. Several authors [9,16 18] also showed that the char particles size influences oxygen diffusion inside the particle which may lead to a non uniform oxygen concentration. Consequently, the combustion temperature, the oxygen partial pressure and the char particles size influence the regime of combustion (i.e. Regime I, II or III).

The most widely used treatment to represent char oxygen reaction is based on a simple global reaction [19 24]:

$$C + \frac{\eta + 2}{2\eta + 2}O_2 \rightarrow \frac{\eta}{\eta + 1}CO + \frac{1}{\eta + 1}CO_2 \quad (1)$$

where η represents the product ratio of CO over CO_2.

However, there has been much controversy in the literature [23] to identify whether the reaction involved is

$$C + \frac{1}{2}O_2 \rightarrow CO \quad (2)$$

followed by CO oxidation in the gas phase to form CO_2, or, alter natively, the reaction may be

$$C + O_2 \rightarrow CO_2 \quad (3)$$

Overall, the authors [25 29] focused on the determination of the CO/CO_2 product ratio in order to determine whether the carbon dioxide is a primary product of the carbon oxygen reaction or a secondary product resulting from the gas phase oxidation of carbon monoxide.

Table 1 summarizes some previous works in regard to the CO/CO_2 product ratio. In these studies, the researchers used several techniques such as low oxygen partial pressures, high gas velocities, gaseous in hibitors and low temperatures of the surrounding gas in order to minimize the CO oxidation in the gas phase. Consequently, they ex clusively measured the heterogeneous reaction between carbon and oxygen. For instance, Tognotti et al. [25] avoided oxidation of CO to

Table 1
Expression of CO/CO_2 product ratio from the combustion of carbon in the literature.

Ref	Carbon type	Reactor	Temperature (K)	P_{O_2} (bar)	Expression CO/CO_2
[25]	Spherocarb char	Electrodynamic balance	670–1670	0.05–1	$50\cdot\exp\left(-\frac{3070}{T}\right)\cdot P_{O_2}^{-0.21}$
[26]	Soot particle	TGA	663–893	0.05–1	$A\cdot\exp\left(-\frac{3200}{T}\right)\cdot P_{O_2}^{-0.27}$
[27]	Graphon	Static system	798–948	$1.3\cdot10^{-5}$ $2.6\cdot10^{-4}$	$A\cdot\exp\left(-\frac{3200}{T}\right)\cdot P_{O_2}^{-0.22}$
[28]	Artificial graphite Coal char	Flow system	733–1173	0.05–0.25	$2500\cdot\exp\left(-\frac{6240}{T}\right)$
[29]	Petroleum coke	Fluidized bed	850–970	0.21	$1340\cdot\exp\left(-\frac{7640}{T}\right)$

CO_2 by heating a single char particle while maintaining the surrounding gas at room temperature. Arthur [28] added $POCl_3$ in the gas stream with the intention of inhibiting the secondary reaction of CO to CO_2. Table 1 also shows that a wide range of carbon types, reactor types and operating conditions were applied. Conclusions drawn from these stu dies can be summarized in several points:

- During carbon combustion, the CO/CO_2 product ratio is constant after a short induction period [25 28].
- Both CO and CO_2 are primary products of the carbon oxygen reac tion.
- The ratio depends on several parameters including the temperature, the oxygen partial pressure, the solid nature and the presence of catalytic impurities.
- For temperatures in the range of 798 948 K and oxygen partial pressures between 0.05 and 1 bar, values of CO/CO_2 ratio vary be tween 0.5 and 6 [25 27].
- There is a general agreement that the ratio increases by raising the combustion temperature.
- The effect of oxygen partial pressure is not well defined. Some workers [28,29] reported no effect of this parameter while others [25 27] observed that the ratio decreases by increasing the oxygen partial pressure.
- Du et al. [26] studied the effect of calcium in the carbon during the combustion. They concluded that the presence of this component strongly favors the formation of CO_2. For instance, at 663 K, the addition of calcium in soot particles decreases the CO/CO_2 product ratio from 0.53 to 0.007. Therefore, one hypothesis is that the CO formation takes place at the carbon edge while the CO_2 production occurs at inorganic sites [26].

More recently, in the case of combustion in fluidized bed reactors, other researchers [30 33] considered that CO is the primary product according to Reaction (2), with the CO diffusing away from the carbon and being converted to CO_2 either immediately above the fluidized bed or in the bubbles rising up through the bed. The CO conversion may be expressed by the following reaction:

$$CO + \frac{1}{2}O_2 \rightarrow CO_2 \tag{4}$$

The simplest way to represent Reaction (2) is that O_2 adsorbs on an active site C() on the carbon surface to give a carbon oxygen complex C(O) which then further desorbs to produce CO [19,30]:

$$\begin{aligned} C + \tfrac{1}{2}O_2 &\rightarrow C(O) \\ C(O) &\rightarrow CO \end{aligned} \tag{5}$$

The different steps in Reaction (5) are known as the Langmuir Hinshelwood formulation which describes the competition between adsorption and desorption phenomena on the char surface.

Hurt and Calo [19] also suggested that the formation of CO_2 may originate from a reaction between carbon oxygen complexes C(O) and gas phase oxygen according to the following reaction:

$$C() + C(O) + O_2 \rightarrow CO_2 + C(O) \tag{6}$$

In the mechanism given by Reactions (5) and (6), any of the steps may be a lumped description of several more elementary steps [19,20].

From the different viewpoints in the literature, it is not clear yet whether the formation of CO_2 originates from a gas phase reaction (i.e. Reaction (4)) or occurs at the solid surface according to Reaction (6).

The kinetic of biomass char combustion was mainly measured using a thermogravimetric analyzer [7,8,10 15,34 37]. This apparatus can continuously record the mass change of a char sample during its com bustion under a well known heating program. In the case of isothermal combustion in TGA, the char sample must undergo a thermal pre treatment before reaching the reaction temperature. Isothermal conditions are then achieved by employing a switching gas method which consists in heating the TGA under an inert atmosphere to the desired temperature before switching the gas from inert to reactive to perform the combustion. After this switching gas method, the newly introduced gas has to diffuse and completely replace the former inert gas in the TGA. It is known that the time necessary for totally replacing the inert gas is likely to affect the char combustion rate as it would cause a continuous change in oxygen concentration. In a previous work [8], it was shown that it required 25 min for the air to totally replace nitrogen after the switching gas method.

The kinetic of char combustion in a fluidized bed reactor has been studied in the case of coal char [30 32] or sewage sludge [33]. The use of a fluidized bed reactor has the advantage of uniform particles mixing, uniform temperature throughout the bed and rapid mass and heat transfers. It also enables a direct feed of the char sample once the reactor has reached the pre set combustion temperature and a steady state. To determine the kinetic of char combustion in a fluidized bed reactor, the produced gases are sampled and their compositions are measured by gas analyzers. Besides, efforts must be made to keep the volume of the sampling gas lines as small as possible. Indeed, the produced gas concentration measured by the analyzer can differ from the one leaving the fluidized bed since the concentration is altered by gas mixing in both the freeboard zone and the sampling lines [32,33]. The response of the analyzer may also modify the produced gas con centration.

Several researchers [11,38,39] observed that the reactivity of char in gasification or combustion is dependent on the type of reactors. For instance, in the case of coal char gasification with CO_2, the authors [38,39] agreed that the reaction rate is higher in the fluidized bed than in the TGA. Zeng et al. [38] explained this phenomenon by the switching gas method in the TGA which leads to a non uniform CO_2 partial pressure at the beginning of the reaction. This non uniform CO_2 partial pressure decreases the char gasification rate. Besides, the au thors also mentioned that the difference in char reactivity in the flui dized bed reactor and in the TGA is less significant at higher gasification temperatures. Mueller et al. [39] also reported that, during the gasifi cation of high volatiles coal char with CO_2 for temperatures above 1073 K, the fluidized bed reactor shows significantly higher carbon conversion rate and reactivity than the TGA. They explained this phe nomenon by thermal annealing during the heat up of the char particles in the TGA which decreases the reactivity. The authors concluded that the knowledge of the thermal history of the particle prior to gasification process is essential for analyzing kinetic data. Finally, Janse et al. [11] studied the difference in combustion reactivity of wood char in two different reactors. They reported that the combustion rate of pine wood char in a packed bed reactor is higher than in a TGA for temperatures up to 648 K. They attributed this difference to the chemisorption of oxygen on carbon which can disturb the weight loss measurement in the TGA. Above a combustion temperature of 648 K, the results of both techniques were found to be similar.

1.1. Brief review on char combustion kinetic

The reactivity of char combustion can be expressed by the rate of a solid state reaction according to the following equation:

$$\frac{dX}{dt} = k(T_p)\cdot h(P_{O_2,s})\cdot f(X) \tag{7}$$

where X, $P_{O_2,s}$ and T_p are the conversion rate, the oxygen partial pres sure at the particle surface (Pa) and the particle temperature (K), re spectively. $f(X)$ is the reaction model also known as the structure function. $h(P_{O_2,s})$ is the oxygen partial pressure function which re presents the effect of oxygen partial pressure on the reaction rate. $k(T_p)$ is the temperature dependent rate constant which is described by the Arrhenius equation:

$$k(T_p) = A \cdot \exp\left(-\frac{E_a}{RT_p}\right) \tag{8}$$

where A is the pre exponential factor, E_a is the activation energy ($J.mol^{-1}$), R is the universal gas constant ($J.mol^{-1}.K^{-1}$). The oxygen partial pressure function can be given in the form of a power law:

$$h(P_{O_{2,s}}) = P_{O_{2,s}}^{n} \tag{9}$$

where n is the reaction order with respect to oxygen.

Many reaction mechanisms have been proposed to represent the carbon oxygen reaction [19]. The most widely used treatment considers Reaction (1) as simple global reaction. The reaction rate is then ex pressed as follows:

$$k(T_p) \cdot h(P_{O_{2,s}}) = R_{global} = A \cdot \exp\left(-\frac{E_a}{RT}\right) \cdot P_{O_{2,s}}^{n} \tag{10}$$

In the literature, most of the authors employed Eqs. (7) and (10) to represent the kinetic of biomass char combustion [8,20]. Nevertheless, in the case of coal char combustion, some researchers [40,41] have used the Langmuir Hinshelwood formulation to represent kinetic data. The simplest Langmuir Hinshelwood formulation takes into account Reaction (5) and is given by:

$$k(T_p) \cdot h(P_{O_{2,s}}) = R_{global} = \frac{k_d k_a P_{O_{2,s}}}{k_a P_{O_{2,s}} + k_d} \tag{11}$$

where k_d and k_a are the rate constants for desorption and adsorption process respectively and follow an Arrhenius law.

Finally, Hurt and Calo [19] considered both Reactions (5) and (6) in the kinetic modelling. They described the kinetic of coal char com bustion by:

$$k(T_p) \cdot h(P_{O_{2,s}}) = R_{global} = \frac{k_a k_6 P_{O_{2,s}}^{2} + k_a k_d P_{O_{2,s}}}{k_a P_{O_{2,s}} + \frac{k_d}{2}} \tag{12}$$

The structure function $f(X)$ represents the reactive surface of the particle. Its evolution during the gasification or combustion reaction is difficult to predict and is subject to discussion in the literature [42]. Due to the complex char structure, several kinetic models are reported in the literature to represent the structure function. The most commonly models used for biomass char combustion are the Power Law Model (PL) and the Volumetric Model (VM) [8,20]. The PL is totally empiric in nature while the VM assumes a homogeneous reaction throughout the particle. In a previous work [8], it was shown that the Grain Model (GM) may also be used to represent kinetic data of biomass char com bustion in TGA. These three models (i.e. PL, VM and GM) are known as deceleratory models which represent a decrease in the reaction rate with conversion. However, during the char combustion or gasification, a bell shape relationship between reaction rate and conversion is fre quently observed. Two different points of view are found. First, in some works [10,21], this curve profile is attributed to a change of the char reactive surface during the reaction. The Random Pore Model (RPM) proposed by Bhatia and Perlmutter [43] has received much interest due to its ability to predict a maximum reaction rate. This model is classi fied as sigmoidal model. It introduces a structural parameter by con sidering that the char particle is porous and the reaction takes place at the internal surface of the pores. As the reaction proceeds, a random overlapping of the pores occurs which can increase or reduce the re active surface area. This model was largely used for gasification of char with CO_2 and steam [21]. A very few authors [10] also found that the Random Pore Model satisfactorily fitted the reaction rate of biomass char combustion. Finally, the second point of view is that the bell shape curve is due to the low gasification agent content in the reactive at mosphere just after switching the gas from inert to reactive [8].

The aim of the present study is to determine the combustion kinetic of a wood char in a fluidized bed reactor. This char was obtained from fast pyrolysis in an annex batch fluidized bed reactor at 923 K and characterized in a previous work [6] to understand its physicochemical properties and reactivity. Experiments are carried out at atmospheric pressure and various temperatures ranging from 603 to 643 K and oxygen partial pressures ranging from 5065 to 21273 Pa.

2. Experimental, material & methods

2.1. Char preparation

The biomass used in this work is a cylindrical beech stick (D = 6 mm, L = 10 mm). A picture of the raw material is given in Fig. 1 (A). The proximate analysis of the biomass was carried out fol lowing the standard test method for chemical analysis of wood charcoal D 1762 84. The results are given in Table 2.

The pyrolysis procedure can be found in detail in a previous work [6]. Briefly, a well known mass of beech sticks is introduced in a batch fluidized bed reactor containing hot inert sand particles. The fast

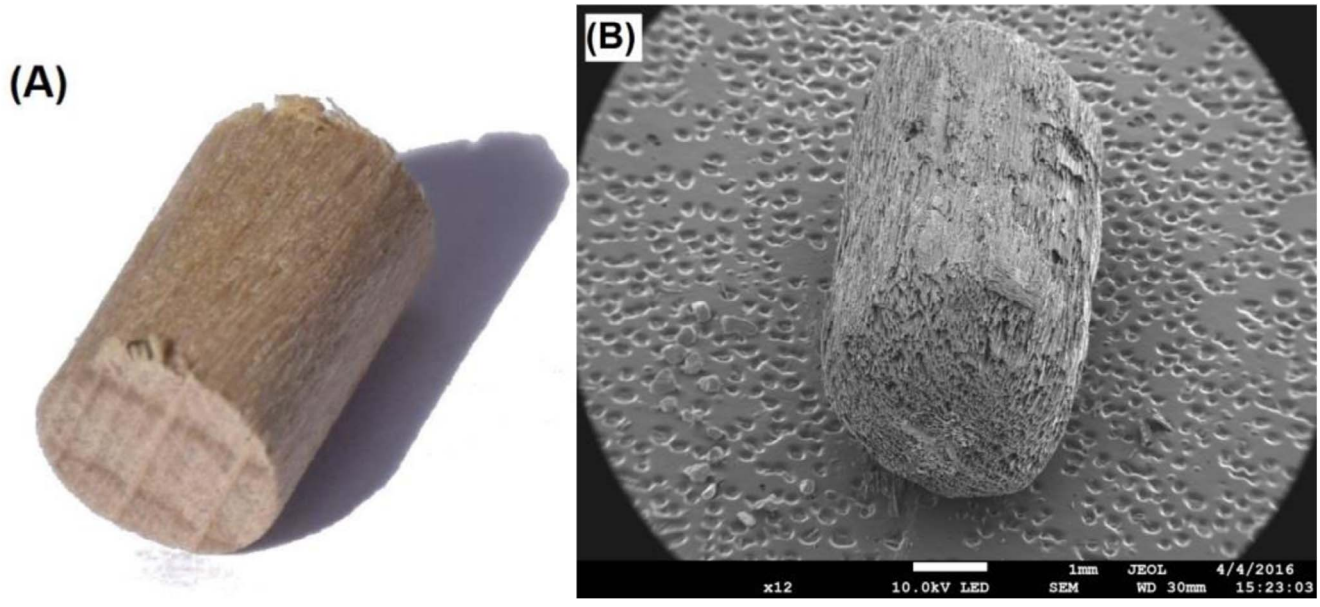

Fig. 1. Picture of the (A) beech stick (STI) and (B) its associated char (called STI650) obtained by pyrolysis at 923 K in a fluidized bed reactor.

Table 2
Proximate analysis of the beech stick (wt%, dry basis).

Biomass	Moisture (%)	Volatile matters (%)	Fixed carbon[a] (%)	Ash (%)
Beech stick	8.40	76.7	14.7	0.2

[a] by difference

pyrolysis of beech sticks is carried out at 923 K under an inert atmosphere of nitrogen at atmospheric pressure. After the pyrolysis, the produced chars (called STI650) are cooled under a flow of nitrogen before being recovered the day after by sieving. A picture of the obtained chars is given in Fig. 1 (B). The soaking time at bed temperature was approximatively 3 h. The produced char is stored inside a pill box until it was analyzed.

Fig. 1 shows that the shape of the produced char particles remained cylindrical close to the initial biomass with a small size decrease (from 5 to 4 mm for the diameter and from 10 to 9 mm for the particle length).

The physical and chemical properties of the beech stick and STI650 are summarized in Table 3. In STI650, the ash is composed of 5.5% of magnesium (Mg), 10.8% of potassium (K), 1.8% of sodium (Na), 30.6% of calcium (Ca) and 51.3% of silica (Si). The apparent density was measured from the weight and volume of five well truncated particles. The true density was obtained by helium pycnometer. The porosity of the biomass and char particles was determined using the following expression:

$$\varepsilon_p = 1 - \frac{\rho_a}{\rho_t} \tag{13}$$

2.2. Char combustion in the fluidized bed reactor

2.2.1. Experimental setup

Isothermal combustion of STI650 was carried out in a fluidized bed reactor. The experimental setup is shown in Fig. 2. The fluidized bed reactor consists of a tube of internal diameter of 5.26 cm and a height of 94 cm heated by an electric furnace (height : 27 cm, inner diameter : 36 cm) delivering 2.6 kW of electric power. About 580 g of olivine are used as fluidized solids with a surface mean diameter (d_{32}) equal to 268 µm and an apparent density (ρ_p) equal to 2965 kg/m^3. The minimum fluidization velocity (U_{mf}) of olivine was measured experimentally and is equal to 5.5 cm/s at 623 K.

The reactor is supplied with nitrogen and air at different proportions according to the combustion operating conditions. The nitrogen and air mass flow rates are carefully regulated by two mass flowmeters Aera FC 7700 CD. The feeding gas is preheated between 200 and 300 °C in a stainless steel tube (inner diameter 1 cm) forming a coil around the reactor. Then, preheated gas enters in a wind box beneath the reactor which is filled with porous silicon carbide (SiC). This structure is used as a mixing zone. The temperature is controlled with a K thermocouple. The gas distribution in the bed is done by a perforated plate of 19 orifices (orifices inner diameter of 1 mm) equipped at its base by a stainless steel sieve with 30 µm of mesh.

The temperature inside the fluidized bed is controlled by two thermocouples located at 5 and 25 cm above the distributor. The former is used to regulate the temperature of the reactor using a PID controller. A differential pressure transmitter is connected at 5 and 500 mm above the distributor in order to follow the pressure drop of the bed. At the reactor outlet, the elutriated particles and condensable gases are collected by a cyclone and a condenser, respectively.

After reaching the operating conditions of the combustion and a steady state regime, a well known amount of char is introduced from the top of the reactor and directly falls down to the surface of the hot fluidized bed.

2.2.2. Sampling method and gas analysis

The sampling of gases is carried out by a stainless steel mobile probe (inner diameter 4 mm) located at the fluidized bed surface. A thermocouple is placed inside the mobile probe to measure the precise temperature at the entrance of the probe. The gas sample is sucked by a vacuum pump connected to a flowmeter (volume flow rate of 100 mL.min^{-1} at STP). At the mobile probe outlet, the pumped gas passes through a cyclone and a filter to separate gas from particles and through a wash bottle cooled at 0 °C to remove any traces of water. To prevent any condensations of steam, all of the lines from the reactor to the entrance of the condensation system are heated to a temperature of 150 °C.

A micro Gas Chromatograph (microGC) Agilent 490 is used to on line analyze the non condensable gases. It is equipped with a Poraplot U 10 m × 0.25 mm ID column connected to a Thermal Conductivity Detector (TCD) calibrated for CO_2 and C_2H_x quantification. A CP Molsieve 5 A 10 m × 0.25 mm column connected to a TCD is calibrated for the analyses and quantification of N_2, H_2, O_2, CO and CH_4. The time lapse between two quantifications is 3 min.

2.2.3. Thermal characterization of the fluidized bed

This section aims to establish the fluidization gas velocity and the char quantity during the experiments which enable the char combustion to occur in isothermal conditions with a constant oxygen partial pressure and a good mixing between olivine and char particles. The experimental results are given in the Supplementary material (A) and led to the following operating conditions:

- A gas velocity of 2.5 times the minimum fluidization velocity to enable a homogeneous temperature in the bed and to avoid any particles elutriation;
- A char sample mass of 2.2 g to perform the combustion in isothermal conditions and a constant oxygen partial pressure;
- A mobile probe located at 27 cm above the distributor to avoid any reactions in the freeboard zone.

2.2.4. Parameters of the study

For each experiment, the composition of the non condensable produced gases was analyzed as a function of time from the continuous micro GC analysis. The total molar flow rate at the outlet of the reactor is given by:

$$\dot{n}_t(t) = \frac{\dot{n}_{N_2}}{x_{N_2}(t)} \tag{14}$$

where $\dot{n}_t(t)$ is the instantaneous total molar flow rate (mol/s), $\dot{n}_{N_2}$ represents the molar flow rate of nitrogen at the entrance of the reactor (mol/s) and $x_{N_2}(t)$ is the measured molar fraction of nitrogen at the

Table 3
Ultimate analysis and properties of the different chars.

	Pyrolysis conditions	Apparent density ρ_a (kg/m^3)	True density ρ_t (kg/m^3)	Solid porosity ε_p (%)	Ultimate analysis (db, wt%)				Chemical Formula
Materials	Pyrolysis Temp. (K)	Direct measurements	He pycnometer	–	C	H	O	Ash	
STICK	–	718 ± 24	1362.5 ± 1	47	44.63	6.37	45.24	0.2	$CH_{1.71}O_{0.76}$
STI650	923	212 ± 32	1589.4 ± 5	87	84.47	2.75	7.39	5.39	$CH_{0.39}O_{0.07}$

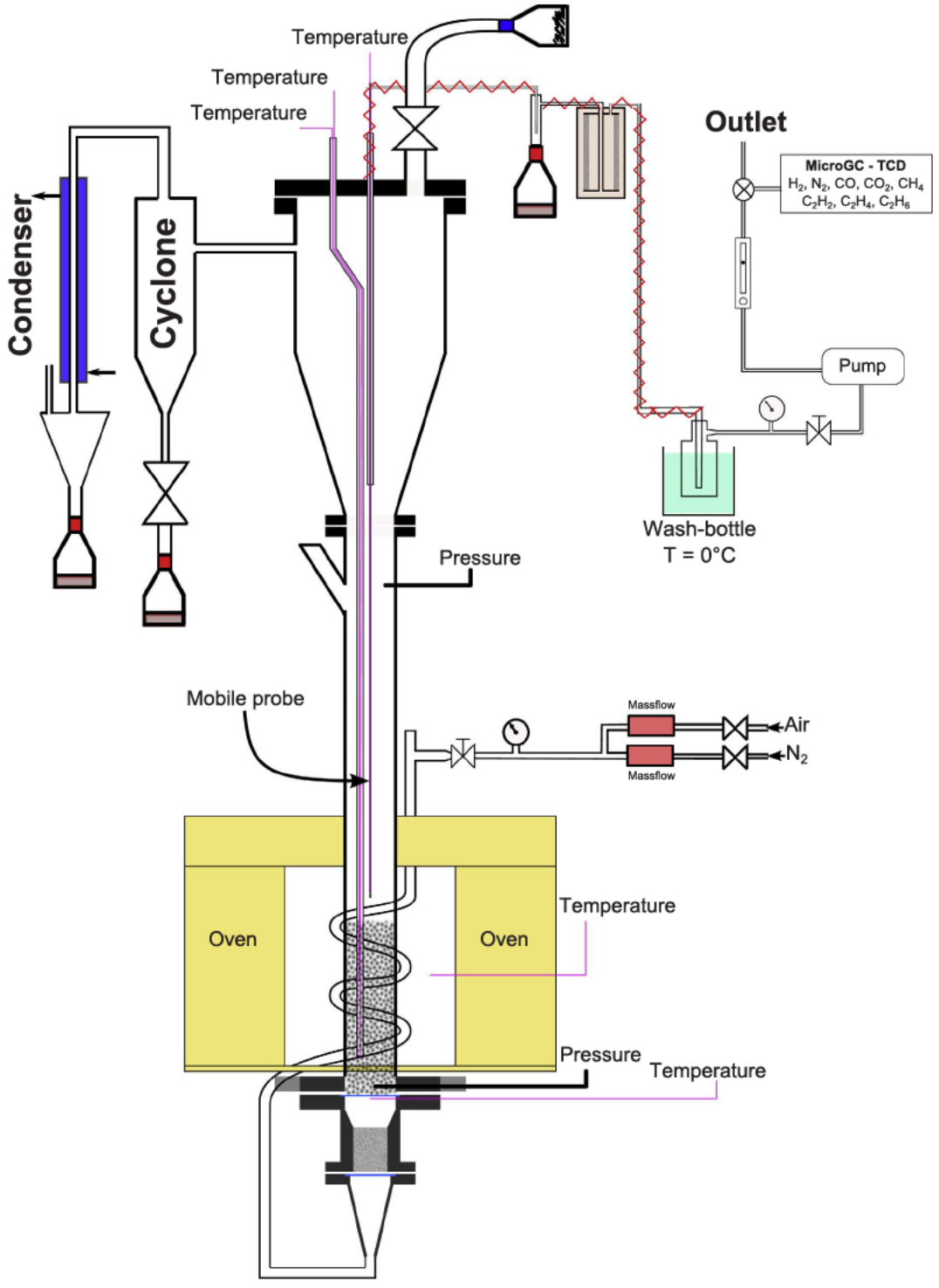

Fig. 2. Experimental setup of the fluidized bed reactor used for char combustion.

reactor outlet.

The partial molar flow rate of each component is calculated as follow:

$$\dot{n}_i(t) = x_i(t) \cdot \dot{n}_t \tag{15}$$

where $\dot{n}_i(t)$ and $x_i(t)$ are the instantaneous partial molar flow rate and molar fraction of component i, respectively. During the combustion, both CO and CO_2 were detected by the gas analyzer.

The carbon conversion rate is determined by the following expression:

$$X_c = \frac{\int_{t=0}^{t} [\dot{n}_{CO}(t) + \dot{n}_{CO_2}(t)]dt}{(n_{carbon})_{char}} \tag{16}$$

where $(n_{carbon})_{char}$ is the amount of introduced carbon in the reactor (mol) and t is the time of the combustion. After each combustion test, the carbon balance was checked and was close to 100%.

The instantaneous combustion rate is obtained using the equation:

$$\frac{dX_c}{dt} = \frac{\dot{n}_{CO}(t) + \dot{n}_{CO_2}(t)}{(n_{carbon})_{char}} \tag{17}$$

Finally, the apparent reaction rate is defined as the derivative of the

evolution of the carbon conversion rate versus time, for a conversion rate of 50%:

$$R_{app} = \left.\frac{dX_c}{dt}\right|_{X=0.5} \quad (18)$$

2.2.5. Experimental measurement errors

Experimental errors were estimated from the gas analyzer calibration and the accuracy of both the gas mass flowmeters and the char mass introduced in the reactor during the combustion. For each gas analysis, the measured values are within an accuracy of 1% with a confidence level of 95%. Consequently, an experimental error of 1% was taken for the components quantification. The mass flowmeters accuracy was fixed to 0.5% of full scale. Regarding the char mass measurement accuracy, the systematic constant error is equal to 0.1 g. Hence, in the following, from these three systematic experimental errors, error bars are introduced into the experimental data.

Besides, some experiments (i.e. combustion at 623 K under air and at 643 K under an oxygen partial pressure of 5065 Pa) have been repeated with a time lapse of 5 months. The results showed a very good repeatability of the replicate experimental measurements.

2.2.6. Response of the reactor and the sampling gas method to a concentration step

The response of the reactor and the sampling gas system to a hydrogen concentration step can be modelled by the association of "n" continuous flow stirred tank reactors in series with the same residence time according to the following expression:

$$\begin{cases} \frac{dY^1_{H_2}}{dt} = \frac{1}{\tau_{CSTR}}\cdot(Y^{in}_{H_2} - Y^1_{H_2}) \\ \frac{dY^2_{H_2}}{dt} = \frac{1}{\tau_{CSTR}}\cdot(Y^1_{H_2} - Y^2_{H_2}) \\ \vdots \\ \frac{dY^n_{H_2}}{dt} = \frac{1}{\tau_{CSTR}}\cdot(Y^{n-1}_{H_2} - Y^n_{H_2}) \end{cases} \quad (19)$$

where $Y^{in}_{H_2}$ is the normalized molar fraction of hydrogen at the inlet of the reactor $(Y^{in}_{H_2} = 1)$, $Y^1_{H_2}...Y^n_{H_2}$ are the normalized molar fractions of hydrogen at the continuous flow stirred tank reactors outlet 1…n, respectively and τ_{CSTR} is the residence time of the continuous flow stirred tank reactors.

The experimental method for determining this transfer function is given in the Supplementary material (B). The parameters n and τ_{CSTR} are identified by solving Eq. (19) using an explicit Runge Kutta (4,5) formula and applying the non linear least squares curve fitting problem. They were found to be 4 and 1 min, respectively. Therefore, the effect of dispersion and gas mixing in the sampling lines can be removed from experimental results by solving Eq. (19) for each experiment.

3. Results and discussions

3.1. Isothermal combustion of STI650 in a fluidized bed reactor

3.1.1. Typical experiment

In this section, the results of a typical experiment are presented. It should be noted that the various findings drawn from this typical experiment are applicable to any other tests.

The results of the combustion of STI650 in a fluidized bed reactor under air at 643 K are presented in Fig. 3 which gives the variation of the molar flow rates of the produced gases CO_2 and CO versus time. First, this figure shows that the molar flow rate of CO_2 is higher than the one of CO. Besides, the molar flow rate of both CO and CO_2 increases before reaching a maximum value followed by a gradual decrease to zero. For each experiment, it was also found that the time corresponding to the maximum molar flow rate is constant and is independent of the combustion temperature. Gomez et al. [44] also observed this maximum during char gasification in TGA. They concluded that this maximum is associated with gas dispersion phenomenon just after switching the gas from inert to reactive in the apparatus. In a fluidized bed reactor, we showed in Section 2.2.6 that the produced gas concentration is affected by gas mixing in the sampling lines. Consequently, the maximum in the molar flow rate is an artefact and depends only on the sampling gas method.

Fig. 4 presents the instantaneous combustion rate versus time for both experimental and corrected results during the combustion under air at 643 K. The effect of gas mixing in the sampling lines leads to a strong difference in the instantaneous combustion rate at the beginning of the reaction. The experimental combustion rate first increases, reaches a maximum and then decreases to zero while the corrected combustion rate gradually decreases.

In the following, the transfer function determined in Section 2.2.6 is used to remove the impact of gas mixing in the sampling lines for each experiment so that only the corrected results are presented.

Fig. 5 emphasizes that the cumulative amount of CO and CO_2 versus carbon conversion rate can be represented by a straight line. Therefore, it can be assumed that the molar flow rates ratio of CO over CO_2 is constant during the combustion and independent of the reaction time and char conversion. This is in good agreement with some authors [25 28] who reported that the ratio CO/CO_2 calculated from the analysis of combustion gases does not change progressively with time. Hence, the CO/CO_2 product ratio was determined from the slopes of the curves of Fig. 5 for each combustion temperature and oxygen partial pressure.

3.1.2. Effect of combustion temperature

The influence of combustion temperature was conducted between 603 and 643 K under a constant oxygen partial pressure of 21273 Pa.

Fig. 6 shows the molar flow rates evolution of CO_2 and CO versus carbon conversion rate during the combustion under air at various temperatures. A raise of the combustion temperature yields to an increase in the molar flow rates of both CO_2 and CO.

The CO/CO_2 product ratio was found to increase by raising the combustion temperature. The results are given in Fig. 7. Our experimental results are much lower than the ones from the literature (see ref [25 27]). This may originate from different points:

- The differences in the type of char and the combustion operating conditions;
- The ash content in STI650 (especially calcium) can catalyze the combustion and increase the formation of CO_2 [26];

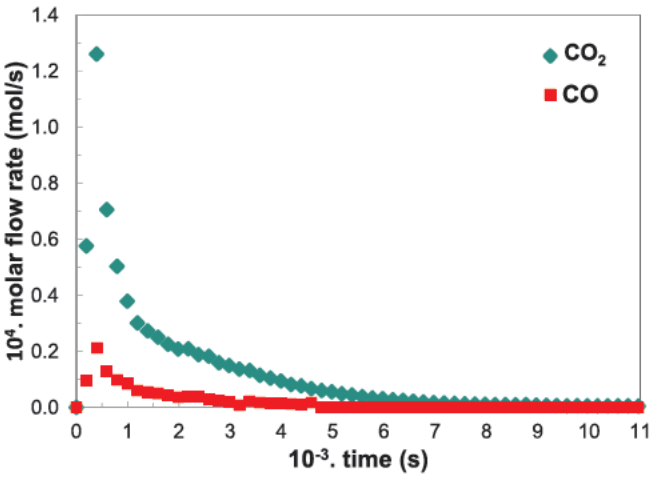

Fig. 3. Molar flow rates of CO_2 and CO during the combustion at 643 K under air.

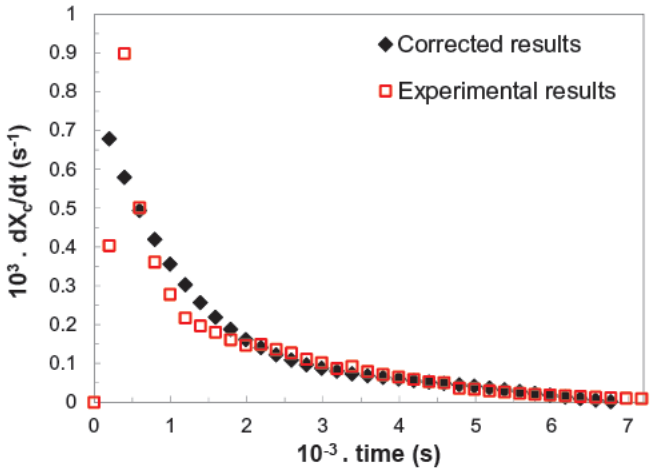

Fig. 4. Comparison between experimental and corrected instantaneous combustion rates during the combustion under air at 643 K.

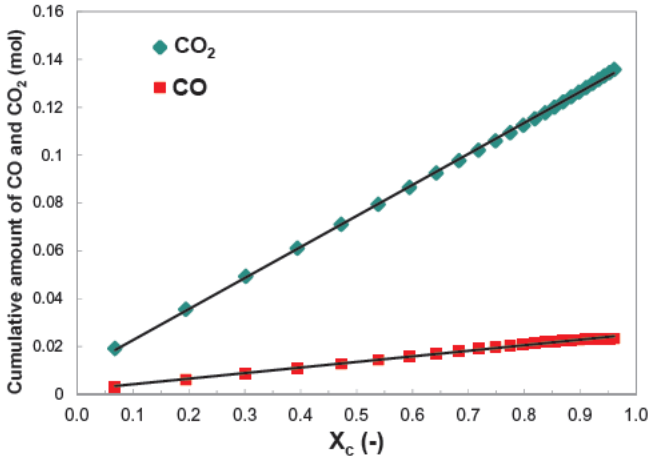

Fig. 5. Cumulative amount of CO and CO_2 versus carbon conversion rate, experiment at 643 K under air.

- The product ratio CO/CO_2 defined in Table 1 is related to the heterogeneous reaction between carbon and oxygen which produces both CO and CO_2. In our case, this ratio also takes into account the oxidation of CO to CO_2 in the gas phase.

However, our experimental data are close to the one obtained from the correlation of Arthur [28] (Fig. 7).

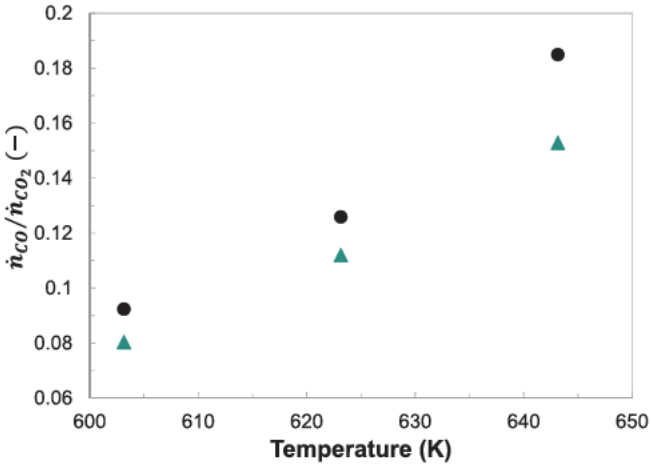

Fig. 7. CO/CO_2 product ratio versus combustion temperature, (●) this work, (▲) Arthur's correlation [28].

Bibliographic works reported that the CO formation during char combustion comes from the heterogeneous reaction between carbon and oxygen (i.e. Reaction (2)). The formation of CO_2 may originate from either the oxidation of CO in the gas phase (i.e. Reaction (4)) or the reaction between oxygen and carbon complex at the solid surface (i.e. Reaction (6)). Consequently, results from Fig. 6 indicate that both the formation of CO and CO_2 are strongly favored with temperature. Besides, results from Fig. 7 emphasize that Reaction (2) is fostered to a higher extent compared to the formation of CO_2.

Fig. 8 (A) presents the effect of combustion temperature on the conversion rate. First, it can be seen that the conversion rate is highly dependent on the combustion temperature. This result is well known in the literature for both the combustion and the gasification of char [7,8,10 15]. For instance, at a given conversion rate of 0.5, it requires a much shorter reaction time at a higher combustion temperature (18 min, 43 min and 113.2 min for temperatures of 643 K, 623 K and 603 K respectively).

Fig. 8 (B) presents the effect of temperature on the instantaneous combustion rate versus conversion. It can be seen that, for each experiment, the combustion rate linearly decreases with conversion rate. Hence, the char reactivity is at its maximum value at the initial stage of the char combustion. In the literature, several kinetic models are used to represent the kinetic of char combustion. Among them, deceleratory models (i.e. VM, PL and GM) may have much interest to represent our experimental data.

Besides, a linear profile was found between the logarithm of

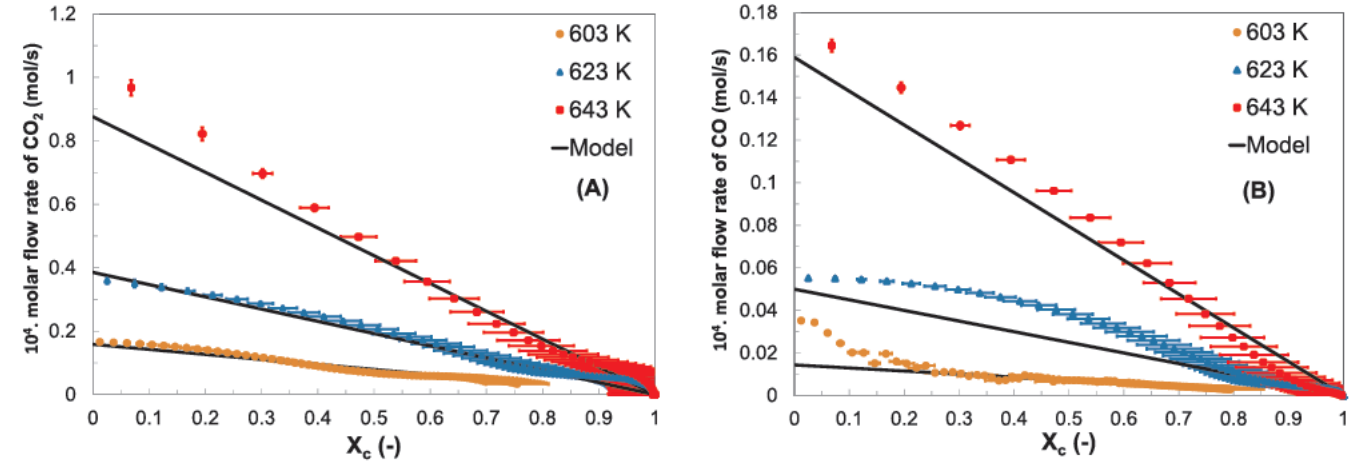

Fig. 6. Effect of combustion temperature under air: (A) molar flow rates of CO_2, (B) molar flow rates of CO.

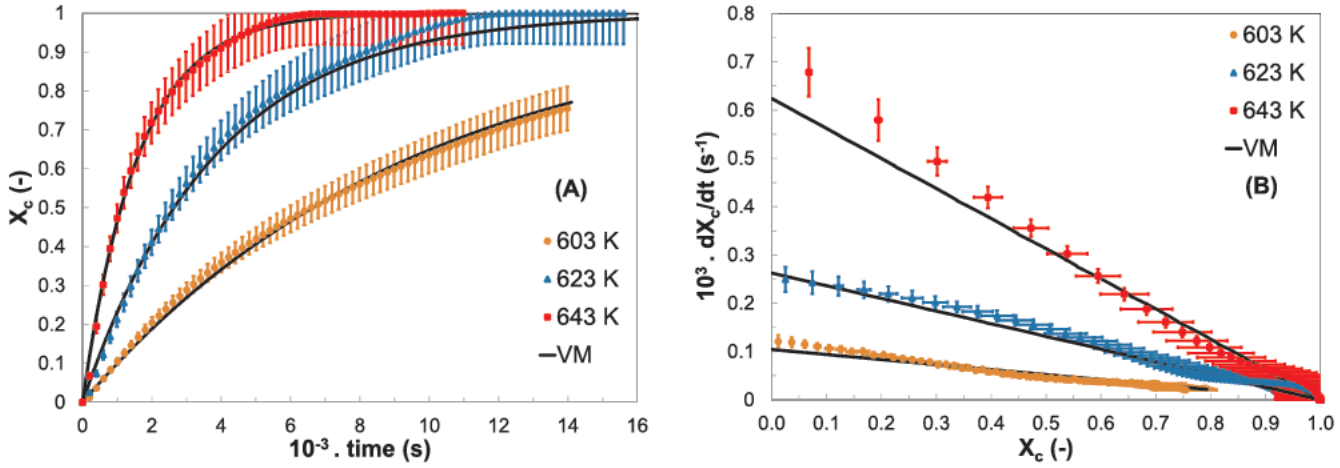

Fig. 8. Effect of combustion temperature under air: (A) conversion rate versus time, (B) instantaneous combustion rate versus conversion rate.

apparent reaction rate versus 1/T. By considering Eqs. (7) and (10) and from the slope of the straight line, the activation energy was determined without considering any reaction models. Its value is equal to 166 kJ/mol and is in the same order of magnitude than previous works in the literature [8,20] indicating that the combustion occurs in Regime I.

3.1.3. *Effect of oxygen partial pressure*

The influence of oxygen partial pressure between 5065 and 21273 Pa was performed at 643 K.

Fig. 9 presents the effect of oxygen partial pressure on the molar flow rates of CO_2 and CO during the combustion at 643 K. An increase in the oxygen partial pressure leads to a higher molar flow rates of both CO and CO_2.

The oxygen partial pressure was found to have no effect on the CO/CO_2 product ratio. This result is highlighted in Fig. 10 which shows that the normalized molar flow rates of CO and CO_2 are constant for conversion rates less than 0.9. This figure also emphasizes that, for each oxygen partial pressure, the CO_2 production is about 9 times higher than the CO production.

The effect of oxygen partial pressure on the carbon conversion rate and the instantaneous combustion rate is highlighted in Fig. 11. It shows that:

- A raise of the oxygen partial pressure leads to a higher combustion rate (Fig. 11 (A));
- A linear evolution of the instantaneous combustion rate versus conversion rate is obtained (Fig. 11 (B)).

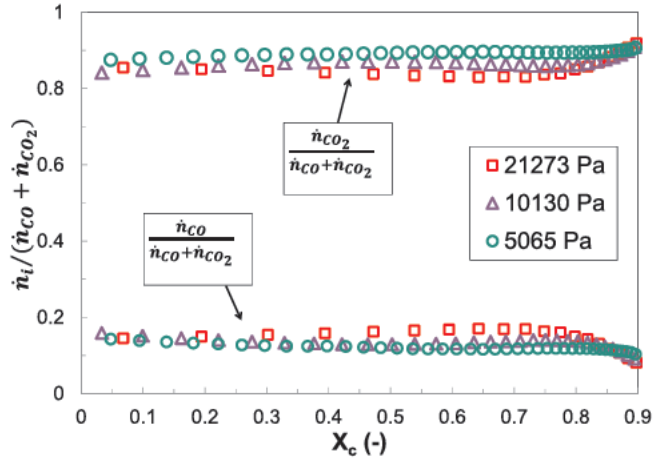

Fig. 10. Normalized molar flow rates of CO and CO_2 versus conversion rate at various oxygen partial pressures and T = 643 K.

Again, we also found a linear evolution between the logarithm of apparent reaction rate versus logarithm of oxygen partial. By considering Eqs. (7) and (10) and from the slope of the straight line, the reaction order with respect to oxygen was equal to 0.73 without considering any reaction model. This reaction order as well as the activation energy determined in Section 3.1.2 are used as initial inputs for

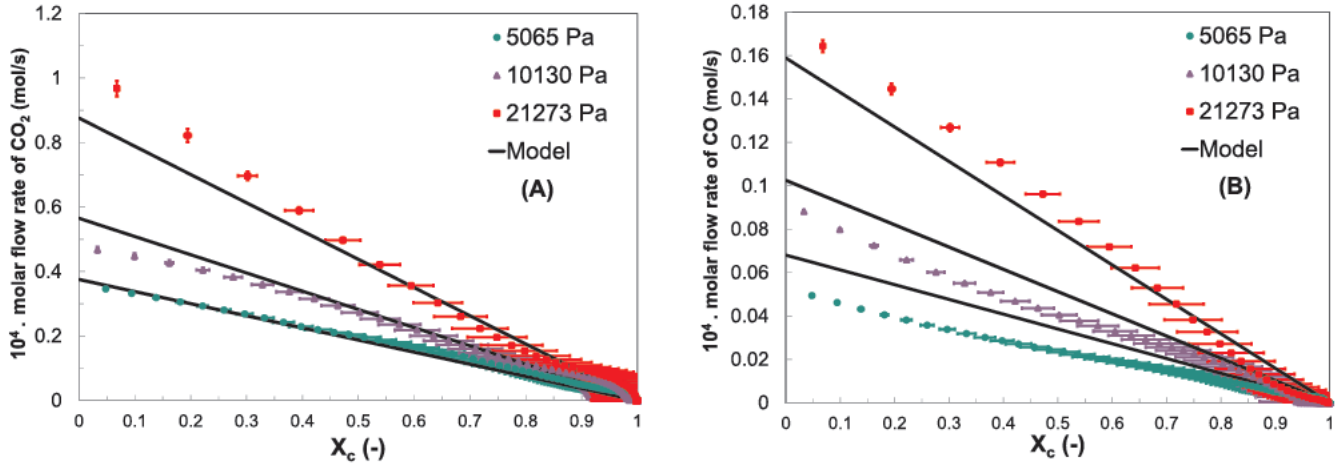

Fig. 9. Effect of oxygen partial pressure at 643 K: (A) molar flow rates of CO_2, (B) molar flow rates of CO.

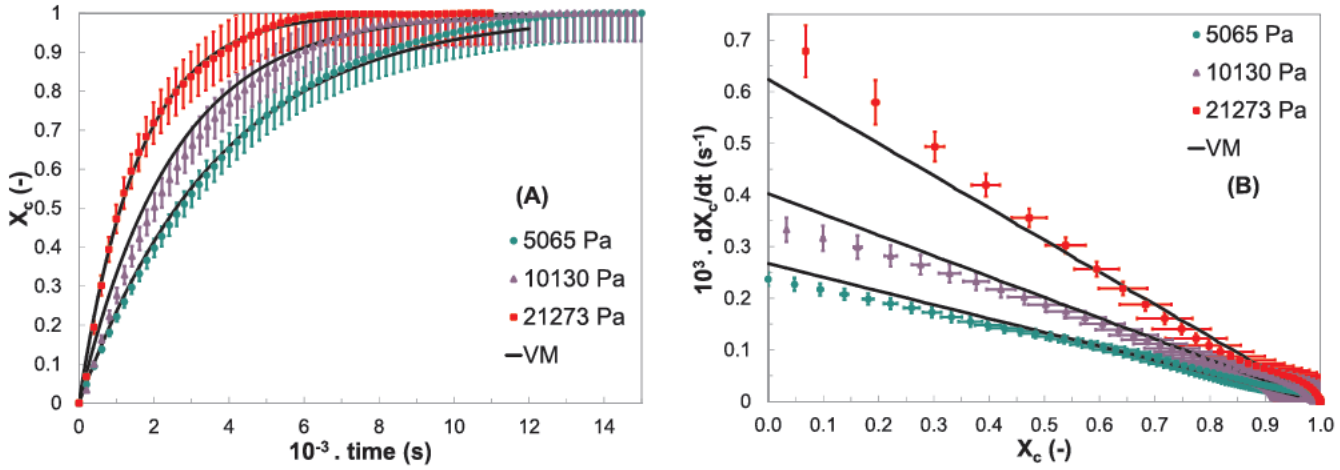

Fig. 11. Effect of oxygen partial pressure at 643 K: (A) conversion rate versus time, (B) instantaneous combustion rate versus conversion rate.

kinetic model optimization.

3.1.4. CO/CO_2 product ratio

We have seen that the CO/CO_2 product ratio increases by raising the combustion temperature while the oxygen partial pressure has no effect on this parameter. In the literature, the authors [25 29] generally represent the ratio according to an expression in the form of:

$$\frac{CO}{CO_2} = A' \cdot \exp\left(-\frac{B'}{T_p}\right) \tag{20}$$

where A' and B' are constant coefficients.

From our results, parameters A' and B' were estimated and Eq. (20) was given by the following expression:

$$\frac{\dot{n}_{CO}}{\dot{n}_{CO_2}} = 6308.8 \cdot \exp\left(-\frac{6724}{T_p}\right). \tag{21}$$

It is important to note that the CO/CO_2 product ratio defined in the literature (Table 1) is related to the heterogeneous reaction between carbon and oxygen which produces both CO and CO_2. In our case, this ratio takes into account both the heterogeneous reaction between carbon and oxygen and the oxidation of CO to CO_2 in the gas phase.

The good agreement observed between our experimental data and the one obtained from the expression of Arthur [28] (see Fig. 7) suggests that Eq. (21) is applicable for a large range of combustion temperatures.

3.2. Kinetic modelling

3.2.1. Kinetic models

In this work, the char is considered as pure carbon for the kinetic modelling. Three deceleratory models were tested (i.e. VM, PL and GM). Since the instantaneous combustion rate showed a linear evolution with conversion rate, the VM was found to be in good agreement with experimental data. This model is presented below.

The Volumetric Model assumes that the reaction takes place uniformly within the volume of the char particle. It is given by the following equation:

$$\frac{dX}{dt} = A_{VM} \cdot \exp\left(-\frac{E_a}{RT_p}\right) \cdot P_{O_{2,s}}^{n} \cdot (1-X) \tag{22}$$

where A_{VM} is the pre exponential factor ($s^{-1}.Pa^{-n}$).

3.2.2. Modelling

To determine kinetic parameters (i.e. pre exponential factor, activation energy and reaction order with respect to oxygen), most of the authors [21] in the literature used a graphitic resolution by integrating Eq. (22) and plotting the left hand side versus time:

$$-\ln(1-X) = K_{VM} \cdot t \tag{23}$$

In this work, the kinetic parameters A_{VM}, E_a and n are estimated by solving Eq. (22) using an explicit Runge Kutta (4,5) formula and applying the nonlinear least squares curve fitting problem. Values of pre exponential factor, activation energy and reaction order with respect to oxygen are given in Table 4. It can be seen that the activation energy is in the same order of magnitude compared to that obtained in Section 3.1.2. Most of literature works on isothermal combustion of biomass and wood char were carried out in TGA [8,20] and the authors found activation energies between 80 and 125 kJ/mol. However, the activation energy found in this work is in good agreement with the study of Adánez et al. [34] who found activation energies ranging from 134 to 142 kJ/mol for isothermal combustion of wood and biomass chars in TGA. Likewise, the reaction order with respect to oxygen is in the same order of magnitude compared to some previous works [8,10,11,34]. Comparisons between experimental data and results obtained from the VM are given in Figs. 8 and 11. A very good agreement is found between experimental data and predicted results.

3.2.3. Reaction scheme during char combustion

In this section, it is assumed that the char combustion in a fluidized bed occurs in two steps:

(1) First the char reacts with oxygen to produce CO according to the heterogeneous reaction in solid phase given in Reaction (2).

The carbon consumption rate r_1 of Reaction (2) is given by the following expression:

$$r_1 = -\frac{dn_c}{dt} = A_{VM} \cdot \exp\left(-\frac{E_a}{RT_p}\right) \cdot P_{O_{2,s}}^{n} \cdot (n_{carbon})_{char} \cdot (1-X) \tag{24}$$

(2) Then the produced CO is partially converted either at the solid surface or in the gas phase to form CO_2 according to Reaction (4).

Table 4
Kinetic parameters obtained with the Volumetric Model by solving Eq. (22), individual confidence limits of 95%.

Char type	A_{VM} ($s^{-1}.Pa^{n}$)	E_a (J/mol)	n (–)	$\min_x \|f(x)\|_2^2$
STI650	901067 ± 150000	144250 ± 2060	0.59 ± 0.02	0.1443

Considering Reactions (2) and (4), the molar flow rates of CO_2 and CO can be expressed by the following equations:

$$\dot{n}_{CO} = r_1 - r_2 \tag{25}$$

$$\dot{n}_{CO_2} = r_2 \tag{26}$$

where r_2 is the rate of Reactions (4).

Combining Eqs. (25) and (26), the molar flow rates of both CO and CO_2 can be calculated:

$$\dot{n}_{CO_2} = r_2 = \frac{-dn_c/dt}{1 + \dot{n}_{CO}/\dot{n}_{CO_2}} \tag{27}$$

where $\dot{n}_{CO}/\dot{n}_{CO_2}$ is estimated from Eq. (21).

Comparisons between experimental molar flow rates of CO and CO_2 and the one obtained from Eqs. (25) and (27) are given in Figs. 6 and 9. A good agreement is obtained. A small difference is observed with results from CO molar flow rates. This may be due to the small amount of CO produced during the combustion which increases the uncertainty, especially at low temperatures and oxygen partial pressures. Consequently, the reaction mechanism given in Reactions (2) and (4) can represent the char combustion in fluidized bed reactor.

3.3. Comparison with TGA results

The isothermal combustion of STI650 in TGA was measured using a TGA Q600 analyzer from TA Instruments. Prior to these tests, the char was grinded to ensure that all particles have approximatively the same diameter equal to 25 µm. Preliminary, tests with various sample weights ranging from 2 to 15 mg showed that 8 10 mg is the optimum sample weight which enables to achieve accurate and repeatable results. Consequently, about 8 mg of STI650 were introduced inside an alumina crucible (inner diameter and height of the crucible equal to 5.5 mm and 4 mm, respectively) for each test. The experimental protocol is divided into two stages. The first one, carried out under high purity nitrogen flow (100 NmL/min), consists of:

- An initial period of 15 min at ambient temperature used to initialize the system;
- A linear heating rate of 10 K/min from ambient temperature to the run temperature;
- A period of 15 min at the run temperature to stabilize the system.

The second stage is the isothermal combustion carried out by switching the nitrogen to a mixture of N_2/O_2 with the same flow rate. Temperatures of 603, 623 and 643 K were tested under air and oxygen partial pressures were varied between 5065 and 21273 Pa at 643 K. All of the gas mixtures of N_2/O_2 have an accuracy of 0.1%. The conversion rate is calculated via the following equation:

$$X = \frac{w_i - w(t)}{w_i - w_{ash}} \tag{28}$$

where w_i, $w(t)$ and w_{ash} are the initial, instantaneous and final sample weight, respectively.

The comparison between results obtained from the char combustion in both reactors showed that, for each operating condition, the char reactivity in fluidized bed is higher compared to TGA. For instance, results from the combustion at 643 K under air are given in Fig. 12. This difference in reactivity between these two reactors was also mentioned by several authors in the literature [38,39] during the char gasification with CO_2.

This difference in char reactivity can originate from several phenomena:

(1) First, during the char combustion in TGA, isothermal conditions are achieved by employing a switching gas method. In a previous paper [8], it was observed that it requires about 25 min to the mixture of N_2/O_2 to completely replace the inert gas in the apparatus after switching the gas from inert to reactive. This leads to significant variation of oxygen partial pressure at the initial stage of the char combustion. For the isothermal combustion of char obtained from pyrolysis of beech bark pellet [8], this effect was taken into account by considering a transfer function which includes two continuous stirred tank reactors in series with a residence time of 3.3 min each. The differential equation system obtained is given by the following expression:

$$\text{TGA Response Time} \begin{cases} \frac{dC_{O_{2,1}}}{dt} = \frac{1}{\tau_{CSTR}} \cdot (C_{O_{2,in}} - C_{O_{2,1}}) \\ \frac{dC_{O_{2,2}}}{dt} = \frac{1}{\tau_{CSTR}} \cdot (C_{O_{2,1}} - C_{O_{2,2}}) \end{cases} \tag{29}$$

where $C_{O_{2,in}}$ is the oxygen concentration at the entrance of the TGA, $C_{O_{2,1}}$ and $C_{O_{2,2}}$ are the oxygen concentrations at the continuous flow stirred tank reactors outlet 1 and 2, respectively and τ_{CSTR} is the residence time of the continuous flow stirred tank reactors.

(2) Second, the presence of diffusional effects within the TGA crucible and char particles may lower the char reactivity in combustion. Indeed, some authors [45 47] observed the presence of a stagnant gas region between the upper surface of the crucible and the surface of the char particles. Diffusional effects in the crucible may be listed as (i) the transfer of oxygen from the upper surface of the crucible to the external layer of the char particles bed, (ii) the diffusion of oxygen through the bed of char particles, (iii) the diffusion of O_2 into the interior of the char particles. In a previous work [8], these transfer effects were modelled by writing the oxygen balance equation in the char layer:

(Accumulation of oxygen in the char layer)
= (Flux of oxygen consumed by the reaction)
+ (Flux of oxygen entering the char layer)

$$\varepsilon \delta_c \cdot S_{crucible} \cdot \frac{dC^s_{O_2}}{dt} = -n_{char,crucible} \cdot \frac{dX}{dt} + S_{crucible} \cdot K_c \cdot (C_{O_{2,2}} - C^s_{O_2}) \tag{30}$$

where ε is the porosity of the char layer ($\varepsilon = 0.4$), $n_{char,crucible}$ is the initial amount of char in the crucible (mol), $S_{crucible}$ is the crucible surface (m^2), $C^s_{O_2}$ and $C^\infty_{O_2}$ are the oxygen concentration at the surface of the char particles and in the bulk, respectively (mol/m^3) and K_c is the global oxygen transfer coefficient (m/s).

Several authors [46] have considered both the diffusion of oxygen through the stagnant zone in the crucible and the diffusion of oxygen in

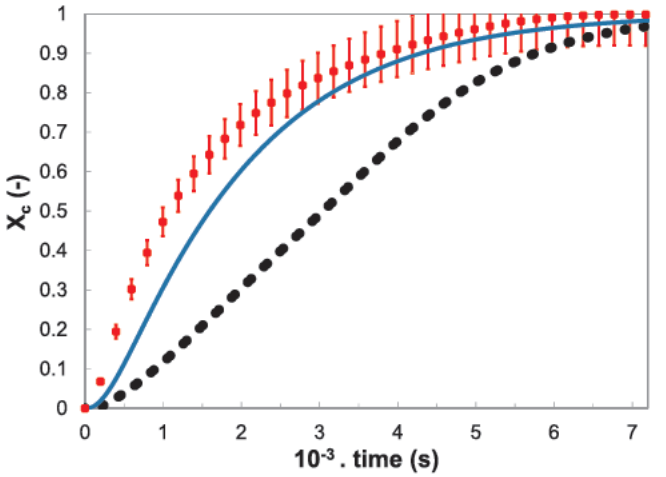

Fig. 12. Combustion at 643 K under air: (■) Fluidized bed reactor, (●) TGA, (—) VM (Eq. (22)) with TGA transfer function (Eq. (29)) and oxygen diffusion in both the stagnant zone and the interstitial space of the char layer (Eqs. (30) and (31)).

the interstitial space within the char layer. This effect is considered by adding a second resistance to oxygen diffusion in the stagnant zone. In this case, the global mass transfer coefficient is expressed using the following equation:

$$K_c = \left(\frac{H - \delta_c}{D_{O_2-N_2}} + \frac{\delta_c}{\varepsilon/\tau \cdot D_{O_2-CO}} \right)^{-1} \quad (31)$$

where D_{O_2-CO} and $D_{O_2-N_2}$ are the diffusion coefficients of oxygen into carbon dioxide and nitrogen respectively (m^2/s). These diffusion coefficients are dependent on the combustion temperature and are calculated from ref [48]. τ is the tortuosity. For fixed bed particles, value of $\tau = \sqrt{2}$ can be assumed [49].

Phenomena (1) and (2) were taken into consideration in order to observe the effect of the TGA transfer function and oxygen diffusion in the crucible. Hence, Eqs. (22), (29) and (30) were solved using an explicit Runge Kutta (4,5) formula. The results are given in Fig. 12. It can be seen that, diffusional effects in the TGA can mostly explain the difference between the fluidized bed and TGA results. However, a non negligible difference in reactivity still remains. This can be explained by the combustion reaction scheme. Indeed, it was shown in Section 3.2.3 that char combustion proceeds through Reaction (2) and Reaction (4). Reaction (2) leads to the formation of a large amount of CO which either diffuses away from char particles and is oxidized to CO_2 in the gas phase or directly reacts with O_2 at the char particle. This oxidation of CO may yield to a significant consumption of O_2 both in the stagnant gas region within the crucible and in the char layer. This CO consumption increases oxygen gradients which decrease the concentration of oxygen entering the char layer and lower the char reactivity in combustion.

Consequently, it appears essential to take into account both mass transfer phenomena within the crucible and CO consumption when determining the kinetic of char combustion in TGA. Otherwise, the kinetic of combustion may be strongly underestimated.

It is important to note that, in addition to mass transfer phenomena within the crucible and CO consumption, the char may also undergo a thermal deactivation due to secondary thermal treatments during the solid heat up under inert atmosphere in the TGA. This effect could lead to a structural ordering of the char and a decrease in its reactivity in combustion [50,51].

4. Conclusion

This paper presented a kinetic study on biomass char combustion in a low temperature fluidized bed reactor. The char was obtained from fast pyrolysis of beech stick in an annex batch fluidized bed reactor at 923 K.

First, the thermal characterization of the fluidized bed was carried out in order to determine the gas velocity and the char sample mass so that isothermal conditions and a constant oxygen partial pressure was achieved during the combustion. The effect of gas mixing in the sampling lines was also thoroughly determined and can be modelled by four continuous flow stirred tank reactors in series with a residence time of 1 min each.

The kinetic study was performed for temperatures up to 643 K, oxygen partial pressures ranging from 5065 to 21273 Pa and cylindrical char particles (D = 4 mm and L = 9 mm). For these operating conditions, the char combustion takes place in Regime I in the absence of any mass transfer limitations.

The kinetic study showed that the Volumetric Model well represents experimental data. The value of activation energy was equal to 144 kJ/mol. Reaction order with respect to oxygen was found to be 0.59. The reaction scheme during the char combustion was defined and indicated that char first reacts with oxygen to form CO which is further oxidized either in the gas phase or directly at the char surface to produce CO_2. Finally, a comparison between kinetic results obtained in a fluidized bed reactor and in TGA demonstrated that both diffusional effects and oxidation of CO in the stagnant zone within the crucible decrease the char reactivity in TGA.

Acknowledgment

The authors thank the « Midi Pyrénées Region » for financial support of this project.

Appendix A. Supplementary data

Supplementary data associated with this article can be found, in the online version, at http://dx.doi.org/10.1016/j.cej.2017.08.063.

References

[1] C. Di Blasi, Modeling chemical and physical processes of wood and biomass pyrolysis, Prog. Energy Combust. Sci. 34 (2008) 47–90.
[2] A. Gómez-Barea, B. Leckner, Modeling of biomass gasification in fluidized bed, Prog. Energy Combust. Sci. 36 (2010) 444–509.
[3] H. Hofbauer, R. Rauch, G. Loffler, S. Kaiser, Six years experience with the FICFB-gasification process, Presented at the 12th European Conference and Technology Exhibition on Biomass for Energy, Industry and Climate Protection, Amsterdam, The Netherland, 2002.
[4] N.M. Laurendeau, Heterogeneous kinetics of coal char gasification and combustion, Prog. Energy Combust. Sci. 4 (1978) 221–270.
[5] J. Szekely, J.W. Evans, H.Y. Sohn, Gas-solid reactions, Academic Press, New York, 1976.
[6] M. Morin, S. Pécate, M. Hémati, Y. Kara, Pyrolysis of biomass in a batch fluidized bed reactor: effect of the pyrolysis conditions and the nature of the biomass on the physicochemical properties and reactivity of the char, J. Anal. Appl. Pyrol. 122 (2016) 511–523.
[7] G. Várhegyi, E. Mészáros, M.J. Antal, J. Bourke, E. Jakab, Combustion kinetics of corncob charcoal and partially demineralized corncob charcoal in the kinetic regime, Ind. Eng. Chem. Res. 45 (2006) 4962–4970.
[8] M. Morin, S. Pecate, E. Masi, M. Hémati, Kinetic study and modelling of char combustion in TGA in isothermal conditions, Fuel 203 (2017) 522–536.
[9] G. Kovacik, A. Chambers, B. Özüm, CO_2 gasification kinetics of two alberta coal chars, Can. J. Chem. Eng. 69 (1991) 811–815.
[10] M. Magnaterra, J.R. Fusco, J. Ochoa, A.L. Cukierman, Kinetic study of the reaction of different hardwood sawdust chars with oxygen. Chemical and structural characterization of the samples, Advances in Thermochemical Biomass Conversion (1993) 116–130.
[11] A.M.C. Janse, H.G. de Jonge, W. Prins, W.P.M. van Swaaij, Combustion kinetics of char obtained by flash pyrolysis of pine wood, Ind. Eng. Chem. Res. 37 (1998) 3909–3918.
[12] C. Di Blasi, F. Buonanno, C. Branca, Reactivities of some biomass char in air, Carbon 37 (1999) 1227–1238.
[13] V. Cozzani, Reactivity in oxygen and carbon dioxide of char formed in the pyrolysis of refuse-derived fuel, Ind. Eng. Chem. Res. 39 (2000) 864–872.
[14] T. Kashiwagi, H. Nambu, Global kinetic constant for thermal oxidative degradation of a cellulosic paper, Combust. Flame 88 (1992) 345–368.
[15] M. Luo, B. Stanmore, The combustion characteristics of char from pulverized bagasse, Fuel 71 (1992) 1074–1076.
[16] S.Y. Zhang, J.F. Lu, J.S. Zhang, G.X. Yue, Effect of pyrolysis intensity on the reactivity of coal char, Energy Fuels 22 (2008) 3213–3221.
[17] N. Standish, A.F.A. Tanjung, Gasification of single wood charcoal particle in CO_2, Fuel 67 (1988) 666–672.
[18] D.P. Ye, J.B. Agnew, D.K. Zhang, Gasification of a South Australian low-rank coal with carbon dioxide and steam: kinetic and reactivity studies, Fuel 77 (1998) 1209–1219.
[19] R.H. Hurt, J.M. Calo, Semi-global intrinsic kinetic for char combustion modeling, Combust. Flame 125 (2001) 1138–1149.
[20] C. Di Blasi, Combustion and gasification rates of lignocellulosic chars, Prog. Energy Combust. Sci. 35 (2009) 121–140.
[21] M.F. Irfan, M.R. Usman, K. Kusakabe, Coal gasification in CO2 atmosphere and its kinetics since 1948: A brief review, Energy 36 (2011) 12–40.
[22] J.C. Wurzenberger, S. Wallner, H. Raupenstrauch, J.G. Khinast, Thermal conversion of biomass: comprehensive reactor and particle modelling, AIChE J. 48 (2002) 2398–2411.
[23] A.N. Hayhurst, M.S. Parmar, Does solid carbon burn in oxygen to give the gaseous intermediate CO or produce CO2 directly? Some experiments in a hot bed of sand fluidized by air, Chem. Eng. Sci. 53 (1997) 427–438.
[24] M.J. Biggs, P.K. Argawal, The CO/CO_2 product ratio for a porous char particle within an incipiently fluidized bed: a numerical study, Chem. Eng. Sci. 52 (1997) 941–952.
[25] L. Tognotti, J.P. Longwell, A.F. Sarofim, The products of the high temperature oxidation of a single char particle in an electrodynamic balance, Twenty-Third Symposium (International) on Combustion, 1990 pp. 1207–1213.
[26] Z. Du, A.F. Sarofim, J.P. Longwell, Kinetic measurement and modelling of carbon oxidation, Energy Fuels 5 (1991) 214–221.

[27] R. Phillips, F.J. Vastola, P.L. Walker Jr., Factors affecting the product ratio of the carbon-oxygen reaction – II reaction temperature, Carbon 8 (1970) 205–210.
[28] J.R. Arthur, Reactions between carbon and oxygen, Trans. Faraday Soc. 47 (1950) 164–178.
[29] T.M. Linjewile, P.K. Agarwal, The product CO/CO2 ratio from petroleum coke spheres in fluidized bed combustion, Fuel 74 (1995) 5–11.
[30] I.M. Bews, A.N. Hayhurst, S.M. Richardson, S.G. Taylor, The order, Arrhenius parameters, and mechanism of the reaction between gaseous oxygen and solid carbon, Combust. Flame 124 (2001) 231–245.
[31] P.S. Fennell, J.S. Dennis, A.N. Hayhurst, The order with respect to oxygen and the activation energy for the burning of an anthracitic char in O_2 in a fluidized bed, as measured using a rapid analyser for CO and CO_2, Proc. Combust. Inst. 32 (2009) 2051–2058.
[32] P.S. Fennell, S. Kadchha, H.Y. Lee, J.S. Dennis, A.N. Hayhurst, The measurement of the rate of burning of different coal chars in an electrically heated fluidized bed of sand, Chem. Eng. Sci. 62 (2007) 608–618.
[33] J.S. Dennis, R.J. Lambert, A.J. Milne, S.A. Scott, A.N. Hayhurst, The kinetics of combustion of chars derived from sewage sludge, Fuel 84 (2005) 117–126.
[34] J. Adánez, L.F. de Diego, F. García-Labiano, A. Abad, J.C. Abanades, Determination of biomass char combustion reactivities for FBC applications by a combined method, Ind. Eng. Chem. Res. 40 (2001) 4317–4323.
[35] A. Zolin, A. Jensen, P.A. Jensen, F. Frandsen, K. Dam-Johansen, The influence of inorganic materials on the thermal deactivation of fuels chars, Energy Fuels 15 (2001) 1110–1122.
[36] Md. Azharul Islam, M. Auta, G. Kabir, B.H. Hameed, A thermogravimetric analysis of the combustion kinetics of karanja (Pongamia pinnata) fruit hulls char, Bioresour. Technol. 200 (2016) 335–341.
[37] C. Branca, C. Di Blasi, Global kinetics of wood char devolatilization and combustion, Energy Fuels 17 (2003) 1609–1615.
[38] X. Zeng, F. Wang, Y. Wang, A. Li, J. Yu, G. Xu, Characterization of char gasification in a micro fluidized bed reaction analyzer, Energy Fuels 28 (2014) 1838–1845.
[39] A. Mueller, H.D. Haustein, P. Stoesser, T. Kreitzberg, R. Kneer, T. Kolb, Gasification kinetics of biomass- and fossil-based fuels: comparison study using fluidized bed and thermogravimetric analysis, Energy Fuels 29 (2015) 6717–6723.
[40] R.H. Essenhigh, Rate equations for the carbon-oxygen reaction: an evaluation of the Langmuir Adsorption Isotherm at atmospheric pressure, Energy Fuels 5 (1991) 41–46.
[41] R.H. Essenhigh, Influence of pressure on the combustion rate of carbon, Twenty-Sixth Symposium on Combustion (1996) 3085–3094.
[42] F. Mermoud, S. Salvador, L. Van de Steene, F. Golfier, Influence of the pyrolysis heating rate on the steam gasification rate of large wood char particles, Fuel 85 (2006) 1473–1482.
[43] S.K. Bhatia, D.D. Perlmutter, A random pore model for fluid-solid reaction: I. Isothermal, kinetic control, AIChE J. 26 (1980) 379–386.
[44] A. Gomez, R. Silberman, N. Mahinpey, A comprehensive experimental procedure for CO2 coal gasification: Is there really a maximum reaction rate? Appl. Energy 124 (2014) 73–81.
[45] P. Ollero, A. Serrera, R. Arjona, S. Alcantarilla, Diffusional effects in TGA gasification experiments for kinetic determination, Fuel 81 (2002) 1989–2000.
[46] S. Schulze, P. Nikrityuk, Z. Abosteif, S. Guhl, A. Richter, B. Meyer, Heat and mass transfer within thermogravimetric analyzer: from simulation to improved estimation of kinetic data for char gasification, Fuel 187 (2017) 338–348.
[47] A. Gómez-Barea, P. Ollero, R. Arjona, Reaction-diffusion model of TGA gasification experiments for estimating diffusional effects, Fuel 84 (2005) 1695–1704.
[48] R.B. Bird, W.E. Stewart, E.N. Lightfoot, Transport phenomena, second ed., Wiley, 2002.
[49] F.A.L. Dullien, Porous Media: Fluid Transport and Pore Structure, second ed., Academic Press, 2012.
[50] A. Zolin, A.D. Jensen, P.A. Jensen, K. Dam-Johansen, Experimental study of char thermal deactivation, Fuel 81 (2002) 1065–1075.
[51] M. Kumar, R.C. Gupta, Influence of carbonization conditions on the gasification of acacia and eucalyptus wood chars by carbon dioxide, Fuel 73 (1994) 1922–1925.